

## Synthesis and Characterization of Dendrimer Templated Supported Bimetallic Pt–Au Nanoparticles

Huifang Lang,<sup>†</sup> Stephen Maldonado,<sup>‡</sup> Keith J. Stevenson,<sup>‡</sup> and Bert D. Chandler<sup>\*†</sup>

Department of Chemistry, Trinity University, One Trinity Place, San Antonio, Texas 78212-7200, and Department of Chemistry, University of Texas at Austin, 1 University Station A5300, Austin, Texas 78712-0165

Received June 11, 2004; E-mail: bert.chandler@trinity.edu

**Abstract:** Bimetallic dendrimer-stabilized nanoparticles (DSNs) were used to prepare supported Pt–Au catalysts within the bulk miscibility gap for this binary system. Hydroxy-terminated generation 5 PAMAM dendrimers were used to prepare Cu<sup>0</sup> nanoparticles (NPs). The Cu<sup>0</sup> NPs were subsequently used to reduce K<sub>2</sub>PtCl<sub>4</sub> and HAuCl<sub>4</sub>, preparing stabilized bimetallic Pt–Au NPs with a 1:1 stoichiometry. The stabilized NPs were adsorbed onto a high surface area silica support and thermally activated to remove the dendrimers. Transmission electron microscopy (TEM), energy dispersive spectroscopy (EDS), and infrared spectroscopy of adsorbed CO showed that this preparation route resulted in NPs in which the two metals are intimately mixed and that the majority of the bimetallic NPs were smaller than 3 nm. Further, the bimetallic NPs were highly active for CO oxidation catalysis near room temperature and showed evidence of CO induced restructuring at ambient temperatures.

### Introduction

Finely dispersed metal NPs, supported on inorganic oxide carriers, are a mainstay of commercial heterogeneous catalysts and are employed in numerous industrial reactions,<sup>1</sup> automotive catalytic converters,<sup>2,3</sup> and fuel cell technologies.<sup>2,4</sup> Bimetallic platinum based catalysts in particular are widely used in industry and for proton exchange membrane (PEM) fuel cells. The discovery of gold based catalysts with extraordinarily high catalytic activity for low-temperature CO oxidation,<sup>5,6</sup> as well as the potential application of gold NPs in catalysis,<sup>7</sup> and nanotechnology<sup>8</sup> have fueled recent interest in gold chemistry and gold based materials.

Supported bimetallic Pt–Au NPs are of similar fundamental interest and importance. The effects of heterometals (e.g., Pt) on the surface chemistry and catalytic properties of gold based NPs are largely unknown.<sup>7</sup> Further, gold is one of only two transition metals more electronegative than platinum,<sup>9</sup> so the incorporation of Au into Pt NPs may have unique effects on catalysis by Pt. Recent interests in the Pt–Au NPs have centered on their optical properties,<sup>10</sup> their potential as selective oxida-

tion<sup>11,12</sup> and dehydrogenation<sup>13</sup> catalysts, electrocatalysts,<sup>14</sup> and selective sensors.<sup>15</sup> Cationic Pt–Au clusters have also recently been shown to have unique reactivity for C–N coupling of methane and ammonia.<sup>16,17</sup>

Silica is an attractive support for studying NP and catalyst properties because it is only mildly acidic, is relatively inert, and has desirable mechanical properties. Gold particles are extremely mobile on silica surfaces<sup>13,18,19</sup> and readily form very large (50+ nm) unreactive particles when treated at elevated temperatures, thus making the preparation of active Au/SiO<sub>2</sub> catalysts difficult.<sup>20</sup> Previous attempts to prepare Pt–Au/SiO<sub>2</sub> catalysts via traditional impregnation methods have resulted in widespread phase segregation and catalysts containing large particle agglomerates.<sup>11,13,21–24</sup> In some cases, the coexistence

<sup>†</sup> Trinity University.

<sup>‡</sup> University of Texas at Austin.

- (1) Poncec, V.; Bond, G. C. *Catalysis by Metals and Alloys*; Elsevier: Amsterdam, 1995; Vol. 95.
- (2) Heck, R. M.; Farrauto, R. J. *Appl. Catal., A* **2001**, *221*, 443–457.
- (3) Bhattacharyya, S.; Das, R. K. *Int. J. Energ. Res.* **1999**, *23*, 351–369.
- (4) Song, C. S. *Catal. Today* **2002**, *77*, 17–49.
- (5) Haruta, M.; Yamada, N.; Kobayashi, T.; Iijima, S. *J. Catal.* **1989**, *115*, 301.
- (6) Haruta, M.; Tsubota, S.; Kobayashi, T.; Kageyama, H.; Genet, M. J.; Delmon, B. J. *Catal.* **1993**, *144*, 175.
- (7) Bond, G. C.; Thompson, D. T. *Catal. Rev. Sci. Eng.* **1999**, *41*, 319–388.
- (8) Daniel, M.-C.; Astruc, D. *Chem. Rev.* **2004**, *104*, 293–346.
- (9) Allred, A. L. *J. Inorg. Nucl. Chem.* **1961**, *17*, 215.
- (10) Shiraishi, T.; Hisatsune, K.; Tanaka, Y.; Miura, E.; Takuma, Y. *Gold Bull.* **2001**, *34*, 129–133.

- (11) Mihut, C.; Descorme, C.; Duprez, D.; Amiridis, M. D. *J. Catal.* **2003**, *212*, 125–135.
- (12) Vazquez-Zavala, A.; Garcia-Gomez, J.; Gomez-Cortes, A. *Appl. Surf. Sci.* **2000**, *167*, 177–183.
- (13) Shen, J.; Hill, J. M.; Ramachandra, M. W.; Podkolzin, S. G.; Dumesic, J. A. *Catal. Lett.* **1999**, *60*, 1–9.
- (14) Lou, Y.; Maye, M. M.; Han, L.; Luo, J.; Zhong, C. J. *Chem. Commun.* **2001**, *5*, 473.
- (15) Skelton, D. C.; Wang, H.; Tobin, R. G.; Lambert, D. K.; Dimaggio, C. L.; Fisher, G. B. *J. Phys. Chem. B* **2001**, *105*, 204–209.
- (16) Koszinowski, K.; Schroder, D.; Schwartz, H. *Organometallics* **2004**, *23*, 1132–1139.
- (17) Koszinowski, K.; Schroder, D.; Schwartz, H. *Angew. Chem., Int. Ed.* **2004**, *43*, 121–124.
- (18) Wolf, A.; Schuth, F. *Appl. Catal., A* **2002**, *226*, 1–13.
- (19) Yang, C.-m.; Kalwei, M.; Schuth, F.; Chao, K.-j. *Appl. Catal., A* **2003**, *254*, 289–296.
- (20) Wolf, A.; Schuth, F. *Appl. Catal., A* **2002**, *226*, 1–13.
- (21) Schwank, J.; Balakrishnan, K.; Sachdev, A. In *New Frontiers in Catalysis: Proceedings of the 10th International Congress on Catalysis*; Solymosi, F., Ed.; Elsevier: Amsterdam, 1993; pp 905–918.
- (22) Chandler, B. D.; Schabel, A. B.; Blanford, C. F.; Pignolet, L. H. *J. Catal.* **1999**, *367*–383.
- (23) Balakrishnan, K.; Sachdev, A.; Schwank, J. *J. Catal.* **1990**, *121*, 441–445.
- (24) Sachdev, A.; Schwank, J. *J. Catal.* **1989**, *120*, 353–369.

of bimetallic Pt–Au NPs was also identified.<sup>13,21,23,24</sup> Bimetallic Pt–Au NPs within the miscibility gap can also be prepared in zeolites by using the zeolite supercages to arrest particle agglomeration and trap bimetallic NPs.<sup>25</sup>

Inorganic and organometallic cluster compounds have also been used to successfully prepare novel bimetallic catalysts.<sup>26</sup> In this route, ligand-stabilized molecular clusters, typically stabilized by CO ligands, are deposited onto oxide supports and thermally activated to remove the ligands. This method has led to the preparation of several bimetallic Pt–Au/SiO<sub>2</sub> catalysts in which the metals are intimately mixed after ligand removal.<sup>11,22,27–29</sup> Unfortunately, the solution chemistry of Pt–Au clusters is dominated by the utilization of phosphine ligands,<sup>30</sup> which are extremely difficult to remove from the ultimate catalyst and are severe poisons for many reactions.<sup>27–30</sup> Several catalysts have also been prepared from an organometallic acetylide-ligated Pt<sub>2</sub>Au<sub>4</sub> cluster.<sup>11,22</sup> These catalysts have shown novel reactivity arising from the intimate mixing of Pt and Au, particularly in hydrocarbon conversion reactions<sup>22,31</sup> and in the selective catalytic reduction of nitrogen oxides.<sup>11</sup> However, Pt:Au metal ratios cannot be varied without an extensive cluster library, which does not exist for nonphosphine Pt–Au clusters.

Recent advances in NP (NP) preparation techniques<sup>8,32,33</sup> offer new opportunities for the preparation of supported bimetallic catalysts. In this process, which is analogous to the cluster route, surface protected mono- or bimetallic NPs are prepared in solution, deposited onto a support, and the colloid stabilizers are removed yielding supported particles with known, characterizable, and reproducible synthetic histories. Because NP compositions may be within bulk miscibility gaps, the colloid method also offers opportunities to prepare and investigate new bimetallic NP catalysts in a rational, controlled fashion. Further, heterogeneous catalysis and some catalyst characterization techniques directly probe the surface chemistry of supported NPs and thus can be considered additional tools in the investigation of NP chemistry and the discovery of new NP properties.

We recently presented a “proof of concept” for this catalyst preparation method using PAMAM dendrimers as NP templates/stabilizers.<sup>34</sup> Dendrimer-stabilized Pt NPs were prepared in aqueous solution, deposited onto a commercial high surface area silica support, and thermally activated to yield supported Pt NPs that were active for CO oxidation and toluene hydrogenation test reactions. These results also showed that PAMAM dendrimers could be completely removed at 300 °C, although the

time required to remove organic residues may vary with metal:dendrimer ratio.<sup>35</sup>

This manuscript describes the development of this general preparative scheme for a new class of bimetallic NP catalysts. Although Pt–Au/SiO<sub>2</sub> system is synthetically challenging to explore, the substantial differences in the surface chemistry of Pt and Au allows for the evaluation of properties that are distinct to each metal. We have also chosen to work well within the miscibility gap as this provides the opportunity to prepare catalysts that are not attainable by traditional routes.

## Results and Discussion

**Preparation and Definition of Materials.** Dendrimer encapsulated Pt or Pd NPs can be prepared by first complexing PtCl<sub>4</sub><sup>2-</sup> ions to the interior amine groups of hydroxyl terminated PAMAM dendrimers, then adding a strong reducing agent (e.g., NaBH<sub>4</sub>).<sup>33</sup> Co-complexation of two metal precursors has led to the preparation of several bimetallic NP systems, including Pt–Pd,<sup>33,36</sup> Pd–Rh,<sup>37</sup> and Pd–Ag<sup>38</sup> NPs. In solution, the Pt–Pd<sup>33,36</sup> and Pd–Rh<sup>37</sup> systems are both active hydrogenation catalysts and exhibit a synergy in catalytic activity that correlates to NP composition.

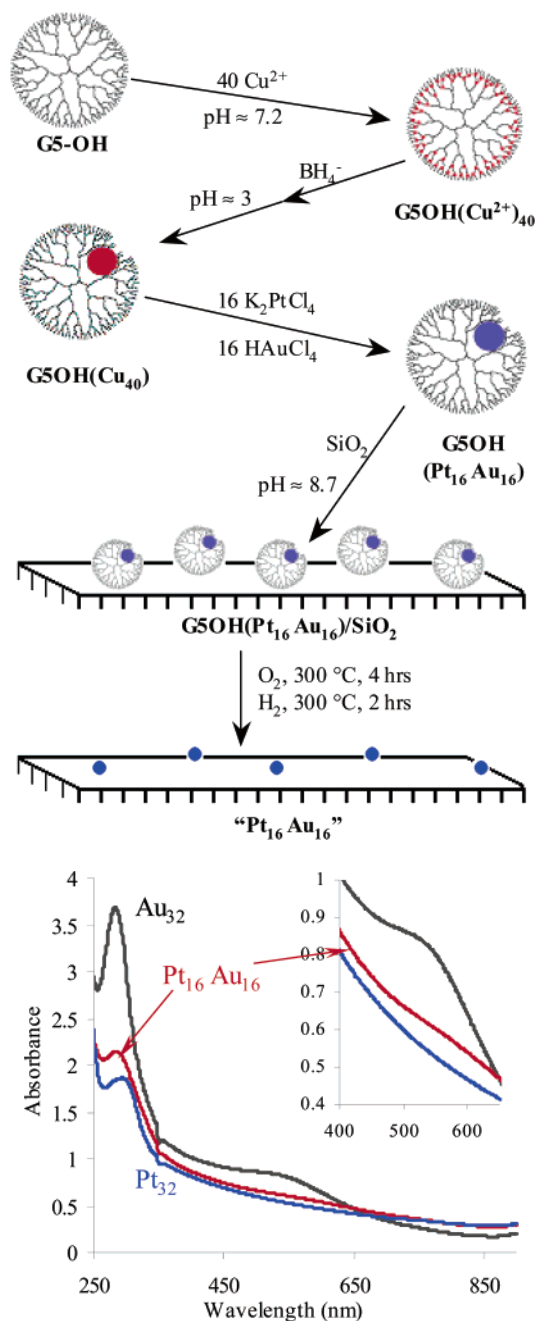
The large standard potential of the aurate ion (+1.00 V vs NHE)<sup>39</sup> makes the preparation of Pt–Au NPs more challenging. Aqueous mixtures of platinum(II) and gold(III) chloride salts are thermodynamically unstable,<sup>39</sup> and gold(III) rapidly oxidizes the Pt(II) complexes appropriate for binding to dendrimer amine groups. Further, Au(III) is not stable in the presence of hydroxyl terminated dendrimers, as it can oxidize the hydroxyl groups (forming larger Au<sup>0</sup> NPs) in the absence of an additional reducing agent.<sup>40,41</sup> To minimize these effects, we have modified a preparative method originally reported by Crooks et al.<sup>42</sup> In this “Cu exchange” method (Scheme 1), Cu NPs are initially prepared under N<sub>2</sub> inside G5-OH PAMAM dendrimers. Oxygen-free solutions of K<sub>2</sub>PtCl<sub>4</sub> and HAuCl<sub>4</sub> are prepared, mixed, and immediately added to the Cu NPs (under nitrogen), utilizing the Cu<sup>0</sup> NPs as an in-situ reducing agent for both Pt and Au. For this study, the final noble metal:dendrimer ratio was held constant (32:1) by adjusting the initial Cu:dendrimer ratio used in NP preparation to account for two- and three-electron reductions of Pt and Au, respectively. The noble metal:dendrimer ratio is well below ratios we<sup>34</sup> and others<sup>43</sup> have used to prepare monometallic Pt and Au DSNs in G5-OH and smaller PAMAM dendrimers.

Figure 1 shows solution UV–vis spectra of G5-OH(Pt<sub>32</sub>), G5-OH(Au<sub>32</sub>), and G5-OH(Pt<sub>16</sub>Au<sub>16</sub>) immediately prior to surface deposition. The Pt-only sample is characterized by a monotonically increasing absorbance at decreasing wavelengths, consistent with literature reports for Pt-dendrimer nanocomposites.<sup>33</sup> The low-energy peak (280 nm) is assigned to an LMCT band

- (25) Riahi, G.; Guillemot, D.; Polisset-Thfoin, M.; Khodadadi, A. A.; Fraissard, J. *Catal. Today* **2002**, *72*, 115–121.  
 (26) Alexeev, O.; Gates, B. C. *Ind. Eng. Chem. Res.* **2003**, *42*, 1571–1587.  
 (27) Chandler, B. D.; Rubinstein, L. I.; Pignolet, L. H. *J. Mol. Catal., A* **1998**, *133*, 267–282.  
 (28) Yuan, Y. Z.; Asakura, K.; Wan, H. L.; Tsai, K. R.; Iwasawa, Y. *J. Mol. Catal., A* **1997**, *122*, 147–157.  
 (29) Yuan, Y. Z.; Asakura, K.; Wan, H. L.; Tsai, K. R.; Iwasawa, Y. *Bull. Chem. Soc. Jpn.* **1999**, *72*, 2643–2653.  
 (30) Pignolet, L. H.; Krogstad, D. A. In *Gold: Progress in Chemistry, Biochemistry, and Technology*; Schmidbaur, H., Ed.; Wiley and Sons: Chichester, U.K., 1999; pp 429–493.  
 (31) Chandler, B. D.; Schabel, A. B.; Pignolet, L. H. *J. Phys. Chem. B* **2001**, *105*, 149–155.  
 (32) Brust, M.; Kiely, C. J. *Colloids Surf., A* **2002**, *202*, 175–186.  
 (33) Crooks, R. M.; Zhao, M.; Sun, L.; Chechik, V.; Yeung, L. K. *Acc. Chem. Res.* **2001**, *34*, 181–190.  
 (34) Lang, H.; May, R. A.; Iversen, B. L.; Chandler, B. D. *J. Am. Chem. Soc.* **2003**, *125*, 14832–14836.

- (35) Lang, H.; May, R. A.; Iversen, B. L.; Chandler, B. D. In *Catalysis of Organic Reactions*; Sowa, J., Ed.; Marcel Dekker: 2004, in press.  
 (36) Scott, R. W. J.; Datye, A. K.; Crooks, R. M. *J. Am. Chem. Soc.* **2003**, *125*, 3708–3709.  
 (37) Chung, Y. M.; Rhee, H. K. *J. Mol. Catal., A* **2003**, *206*, 291–298.  
 (38) Chung, Y. M.; Rhee, H. K. *J. Colloid Interface Sci.* **2004**, *271*, 131–135.  
 (39) Latimer, W. M. *The Oxidation States of the Elements and their Potentials in Aqueous Solutions*, 2nd ed.; Prentice-Hall: New York, 1953.  
 (40) West, R.; Wang, Y.; Goodson, T. *J. Phys. Chem. B* **2003**, *107*, 3419–3426.  
 (41) Esumi, K.; Hosoya, T.; Suzuki, A.; Torigoe, K. *Langmuir* **2000**, *16*, 2978–2980.  
 (42) Zhao, M. Q.; Crooks, R. M. *Chem. Mater.* **1999**, *11*, 3379–3385.  
 (43) Kim, Y.-G.; Oh, S.-K.; Crooks, R. M. *Chem. Mater.* **2004**, *16*, 167–172.

Scheme 1



**Figure 1.** UV-vis spectra for Pt<sub>32</sub> (blue), Au<sub>32</sub> (black), and Pt<sub>16</sub>Au<sub>16</sub> (red) DSNs in solution.

from residual Cu(II)-dendrimer complexes.<sup>33</sup> The Au-only sample has similar features with an additional shoulder from 500 to 600 nm. This shoulder is consistent with the plasmon band arising from Au NPs larger than 2 nm.<sup>43,44</sup> The bimetallic Pt<sub>16</sub>Au<sub>16</sub> spectrum is generally similar to the spectrum of Pt<sub>32</sub> and the Au-plasmon band around 530 is not present. There is also a very weak shoulder at around 600 nm that correlates very well with the visible ligand-field transitions in Cu(II)-dendrimer complexes.<sup>33</sup> We cannot rule out the possibility that this band is due to the presence of larger Au agglomerates, although we found no evidence for such species in our TEM studies (*vide infra*).

(44) Alvarez, M. M.; Khoury, J. T.; Schaaff, T. G.; Shafiqullin, M. N.; Vezmar, I.; Whetten, R. L. *J. Phys. Chem. B* **1997**, *101*, 3706–3712.

**Table 1.** Catalyst Preparation and Characterization Data

	Pt <sub>32</sub>	Au <sub>32</sub>	Pt <sub>16</sub> Au <sub>16</sub>	Pt <sub>32</sub> +Au <sub>32</sub>
nominal Cu:dendrimer <sup>a</sup>	32	48	40	32, 48
Pt loading (wt. %) <sup>b</sup>	0.25%		0.14%	0.14%
Au loading (wt. %) <sup>b</sup>		0.29%	0.15%	0.15%
Pt:Au ratio <sup>c</sup>			15:17	15:17
<i>d</i> <sub>ave</sub> (nm) <sup>d</sup>	3.3	14.5	2.6	4.2
standard deviation <sup>e</sup>	0.8	14.8	1.1	4.2
<i>d</i> <sub>MP</sub> (nm) <sup>f</sup>	3.5	12	2.0	3.0

<sup>a</sup> Cu:dendrimer stoichiometry. <sup>b</sup> Supported catalyst % Pt and Au, determined by atomic absorption spectroscopy. Cu content was also measured for all catalysts and was always below detection limits (0.01%). <sup>c</sup> Determined from Pt and Au loadings. <sup>d</sup> Arithmetic mean diameter of all imaged particles. <sup>e</sup> Standard deviation in *d*<sub>ave</sub>. <sup>f</sup> Most probable diameter: The observed particle diameter that occurs with the highest frequency, i.e., the highest bar on the PSDs in Figure 2. This quantity allows offers an additional means of comparing different types of distributions (e.g., Gaussian vs Maxwell–Boltzman).

The dendrimer-stabilized NPs (DSNs) are then adsorbed onto silica<sup>34</sup> and washed with EDTA solution to remove the remaining Cu. Numerous washing techniques were evaluated; the protocol described here always resulted in Cu content below detection limits (0.01% Cu). The supported DSNs were activated under flowing O<sub>2</sub> (300 °C, 4 h) followed by reduction with flowing H<sub>2</sub> (300 °C, 2 h). This thermolysis treatment has previously been shown to remove PAMAM dendrimers from silica supported monometallic Pt DSNs without causing measurable particle agglomeration.<sup>34</sup> It is possible that some organic residues remain after the standard pretreatment; however, this activation protocol removes 95+% of the C and N<sup>34</sup> and provides a reasonable starting point for evaluating new catalysts.

Using this general preparative scheme, a substantial number of compositionally important factors (beyond the Pt:Au and metal:dendrimer ratios) can be varied. The total metal loading metal:dendrimer ratio and dendrimer loading are important parameters for the deposition and activation of DSNs; maintaining consistent dendrimer loadings is particularly important for comparing dendrimer derived catalysts.<sup>34,35</sup> For this study, the final metal:dendrimer ratio was held constant (32:1) and silica masses were adjusted to fix both the total metal (ca. 0.3 wt. % metal) and dendrimer loading. Final metal ratios were determined by atomic absorption (AA) spectroscopy (Table 1) and were always close to the expected values. The Pt:Au ratio was initially set to be approximately 1:1, as this ratio is within the bulk miscibility gap and represents a metal ratio not available through cluster precursors.

For comparison, three additional materials were prepared. We have chosen a nomenclature system that indicates the stoichiometric metal:metal and metal:dendrimer ratios used in catalyst preparation. The primary material of interest is termed the bimetallic catalyst defined as Pt<sub>16</sub>Au<sub>16</sub>. The monometallic Pt and Au materials (Pt<sub>32</sub> and Au<sub>32</sub>, respectively) were prepared to evaluate the behavior of each metal in the absence of the other. An additional advantage of the dendrimer route for bimetallic catalyst preparation is that it offers the opportunity to prepare an additional control material containing both metals. Consequently, we individually prepared monometallic Pt and Au NP solutions via Cu displacement, combined them, and simultaneously deposited them on to silica. We describe this material (Pt<sub>32</sub>+Au<sub>32</sub>) as a “cometallic” to distinguish it from the “bimetallic” Pt<sub>16</sub>Au<sub>16</sub>. Although both materials contain both metals with the same metal ratios and loadings, Pt<sub>32</sub>+Au<sub>32</sub> has

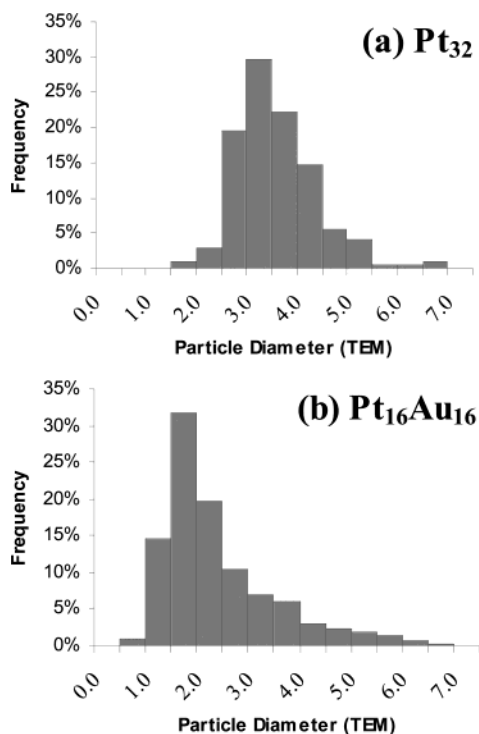


**Figure 2.** TEM particle size distributions for Pt<sub>32</sub> and Pt<sub>16</sub>Au<sub>16</sub>.

been intentionally prepared to have little or no interactions between the monometallic NPs. In contrast, the bimetallic Pt<sub>16</sub>Au<sub>16</sub> has been prepared with the goal of forming bimetallic NPs in which Pt and Au are intimately mixed.

**Transmission Electron Microscopy.** Table 1 includes bulk characterization data for all four materials, as well as a summary of the TEM data. Representative particle size distributions (PSDs) for Pt<sub>32</sub> and Pt<sub>16</sub>Au<sub>16</sub> are shown in Figure 2. Additional PSDs and representative TEM micrographs are provided in the Supporting Information. Particle sizes for Pt<sub>32</sub> are larger than those observed for catalysts prepared by direct complexation<sup>34</sup> and suggest that Cu displacement leads to Pt NPs stabilized by several dendrimers. The particles on Au<sub>32</sub> are substantially larger with 15% of the observed particles larger than 20 nm. This indicates that sintering is a substantial problem for Au/SiO<sub>2</sub> catalysts, consistent with literature reports.<sup>13,18,19</sup> The Pt<sub>32</sub>+Au<sub>32</sub> PSD contains features of the PSDs from both monometallic catalysts, although the most probable diameter ( $d_{MP}$ ) is slightly lower than for Pt<sub>32</sub>. A similar effect has been reported for Pt–Au/SiO<sub>2</sub> catalysts prepared from the impregnation of chloride salts, suggesting that the presence of Au affects Pt particle sizes by preventing the formation of large Pt particles.<sup>21–24</sup>

TEM studies of Pt<sub>16</sub>Au<sub>16</sub> indicate that the particles are substantially smaller than the other catalysts. The Pt<sub>16</sub>Au<sub>16</sub> PSD is similar to a Maxwell–Boltzmann distribution, making the most probable diameter ( $d_{MP}$ ) a more practical tool for describing the majority of the imaged particles. Notably, 75% of the imaged particles were smaller than 3 nm. No particles larger than 7 nm were observed, in striking contrast to the other Au containing materials, suggesting that the Cu exchange synthesis leads to bimetallic particles that are substantially more resistant to sintering than monometallic Au.

Pt<sub>16</sub>Au<sub>16</sub> was also examined with X-ray energy dispersive spectroscopy (EDS) during high-resolution TEM experiments (Figure 3). The average Pt composition (14 measurements) was

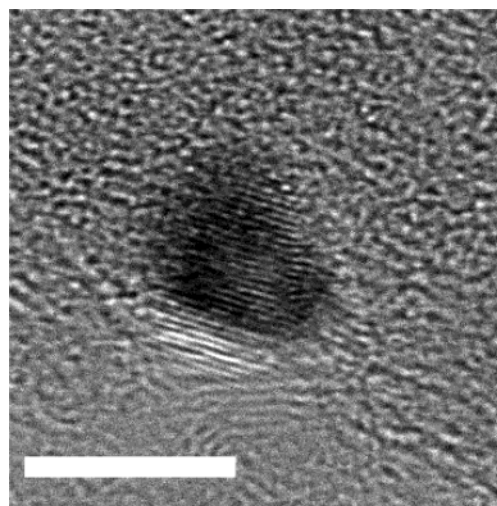


**Figure 3.** High-resolution TEM image from Pt<sub>16</sub>Au<sub>16</sub>. Scale bar is 5 nm.

40% Pt with a 25% standard deviation. This value is in reasonable agreement with the bulk AA measurements for the catalyst (48% Pt), especially considering that that EDS measurements are difficult to calibrate because of lack of available standards. However, EDS alone is insufficient to properly identify the nature of elemental distribution of small particles. Further electron beam diffraction studies are necessary to differentiate between a phase-segregated platinum/gold composition from a homogeneous distribution of platinum and gold atoms. Nevertheless, the analysis presented here represents strong evidence for the bimetallic nature of the Pt<sub>16</sub>Au<sub>16</sub> NPs.

**Infrared Spectroscopy.** Infrared spectroscopy of adsorbed CO is an important characterization tool for NPs as it directly probes their surface features. Figure 4 shows IR spectra of CO adsorbed on the Pt containing materials. No CO adsorption was detected on Au<sub>32</sub> (spectrum in Supporting Materials), consistent with large Au particles being chemically inert.<sup>7</sup> In Figure 4a, the infrared spectrum of CO adsorbed on Pt<sub>32</sub> shows a strong absorption band at 2085 cm<sup>-1</sup>, consistent with supported Pt catalysts<sup>45</sup> and with other dendrimer derived Pt catalysts.<sup>34</sup> The IR spectrum of Pt<sub>32</sub>+Au<sub>32</sub> (Figure 4c) largely resembles that of Pt<sub>32</sub>. It is somewhat less symmetric, with tailing at lower energies. This asymmetry suggests that most surface sites are consistent with Pt NPs. However, the asymmetry also suggests that there is some degree of surface site heterogeneity that is distinct from the monometallic Pt material.

IR spectra of Pt<sub>16</sub>Au<sub>16</sub> (Figure 4b) are substantially different from Pt<sub>32</sub> and Pt<sub>32</sub>+Au<sub>32</sub> and are consistent with the preparation of highly dispersed supported, intimately mixed bimetallic NPs.<sup>11,22</sup> Immediately noticeable is the high-energy absorption band (2113 cm<sup>-1</sup>), which is consistent with CO bound to Au surface sites and supports the existence of bimetallic NPs.<sup>11,13,27</sup> Further, this peak clearly shows that a substantial fraction of the Au atoms is reactive and capable of binding CO. The CO giving rise to this band is bound weakly to the surface and slowly desorbs with continued purging at room temperature. This desorption is responsible for the continued observation of gas-phase CO (periodic oscillations below 2143 cm<sup>-1</sup>). On the basis of the amplitude of these oscillations, the gas-phase concentration of CO is approximately 10 ppm.

(45) Hollins, P. *Surf. Sci. Rep.* **1992**, *16*, 51.

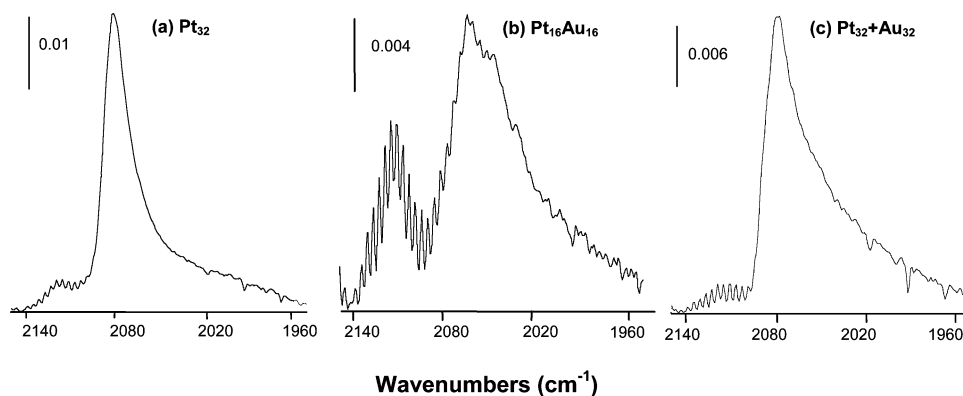


**Figure 4.** Infrared spectroscopy of CO adsorbed at 30 °C on (a) Pt<sub>32</sub>, (b) Pt<sub>32</sub>+Au<sub>32</sub>, and (c) Pt<sub>16</sub>Au<sub>16</sub>.

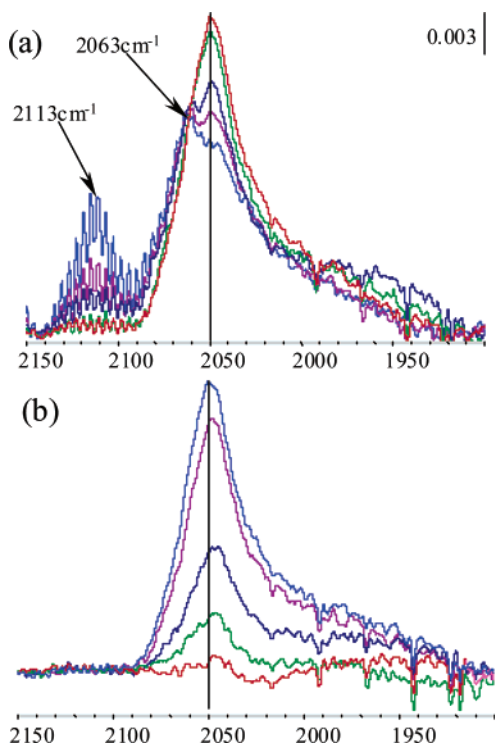


**Figure 5.** Infrared spectroscopy during CO desorption from Pt<sub>16</sub>Au<sub>16</sub> (a) 30 [blue], 70, 90, and 120 [red] °C and (b) 120 [blue], 150, 170, 180, and 190 [red] °C

The lower energy band in Figure 4b (2063 cm<sup>-1</sup>) is consistent with CO bound Pt, as it is strongly bound to the surface and is not readily removed at room temperature. This band is broader than the peak on Pt<sub>32</sub> or on other dendrimer derived Pt NPs<sup>34</sup> and red shifted 20 cm<sup>-1</sup> relative to CO on monometallic Pt NPs. This result is also consistent with the presence of a bimetallic surface, where surface Pt atoms are diluted in Au. The physical separation of diluted Pt–CO dipoles would reduce their ability to participate in dipole coupling, resulting in an apparent red shift relative to a pure Pt surface.<sup>45</sup>

The spectra in Figure 4 were recorded after dosing the samples with CO at room temperature and flushing the gas-phase CO from the sample chamber with flowing helium. Heating the sample while continuing to flush with He (Figure 5) caused further change to the infrared spectrum. In Figure 5a, Au–CO band disappears quickly, consistent with CO being weakly bound to Au on silica supported Pt–Au NPs. The disappearance of the Au–CO band also coincides with an increase in the Pt–CO band intensity. In contrast, when Pt<sub>32</sub> is

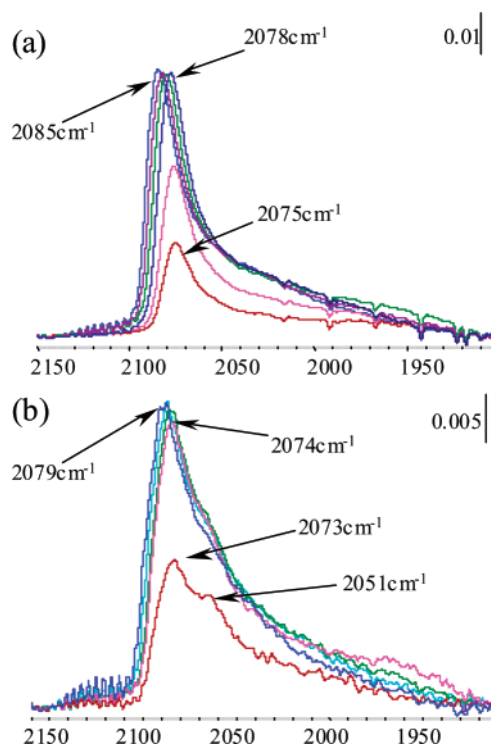


**Figure 6.** Infrared spectroscopy during CO desorption from (a) Pt<sub>32</sub> 30 [blue], 70, 100, 130, 140, and 145 [red] °C and (b) Pt<sub>32</sub>+Au<sub>32</sub> (40 [blue], 70, 100, 110, 115 [red] °C)

heated to desorb CO (Figure 6), this stretching frequency shifts from 2085 cm<sup>-1</sup> to 2075 cm<sup>-1</sup> because of decreased coupling between adsorbed CO molecules.<sup>45</sup> The band intensity is relatively constant until the temperature reaches 140 °C and CO rapidly desorbs from the surface. Infrared spectra of Pt<sub>32</sub>+Au<sub>32</sub> largely resemble Pt<sub>32</sub> spectra, with the exception of a small shoulder at approximately 2050 cm<sup>-1</sup>. This shoulder may suggest the presence of some bimetallic sites (vide infra) and that a small fraction of the Pt has been incorporated into Au particles.<sup>11,22,23</sup>

Closer inspection of the Pt<sub>16</sub>Au<sub>16</sub> desorption experiment suggests that the broad room-temperature Pt–CO band may be better described as two bands at 2065 and 2050 cm<sup>-1</sup>. Upon heating the sample, changes in the Pt–CO band are due to a substantial increase in the intensity of the 2050 cm<sup>-1</sup> band. Once CO completely desorbs from Au, the Pt–CO band becomes substantially more symmetric and the 2065 cm<sup>-1</sup> band is no longer distinguishable. Complete desorption of the 2050 cm<sup>-1</sup> band also occurs at a substantially higher temperature than with

the Pt<sub>32</sub> or Pt<sub>32</sub>+Au<sub>32</sub> samples, suggesting that CO is more strongly bound to the well mixed bimetallic NPs.

We believe that this phenomenon is best explained by a CO induced restructuring of the Pt–Au NPs. Au has a lower work function than Pt and, in the absence of ligands, Au is more stable at the surface of Pt–Au alloys or bimetallic NPs.<sup>46,47</sup> However, CO forms strong bonds with Pt<sup>0</sup> and provides a driving force for pulling Pt to the particle surface.<sup>46</sup> The fluxional behavior of Pt NPs has also been suggested by Somorjai and co-workers.<sup>48</sup> For Pt<sub>16</sub>Au<sub>16</sub>, this restructuring appears to be an activated process near room temperature, as increasing temperature provides the energy required to rearrange the NP and draw Pt to the surface.

Similar behavior has been suggested for dilute alloys of Pt in Au.<sup>13,46</sup> In particular, Dumesic and co-workers have examined CO adsorbed on a supported Pt–Au/SiO<sub>2</sub> catalyst prepared with metal ratios in the miscibility range.<sup>13</sup> Their method prepared bimetallic Pt–Au NPs of 2–5 nm in diameter, which coexisted with numerous large (ca. 200 nm) Au particles. Infrared spectra of CO adsorbed on their catalyst indicated a predominantly Au surface at 203 K. Although no restructuring was observed, adsorption at ambient temperatures indicated that the surface was substantially enriched in Pt relative to the low-temperature spectrum. The room-temperature spectra reported by Dumesic's group<sup>13</sup> are also consistent with spectra for CO adsorbed on Pt–Au NPs prepared from organometallic clusters.<sup>11,22,49,50</sup>

The mobility of Pt and Au within the bimetallic NPs may also help to explain why the particles on Pt<sub>16</sub>Au<sub>16</sub> remain small after fairly forcing activation conditions (8 h at 300 °C). The incorporation of Pt into the NP clearly anchors Au to the support, preventing the severe particle agglomeration that is so prevalent in monometallic Au/SiO<sub>2</sub> catalysts.<sup>13,20,24,49</sup> The apparent mobility of Pt atoms within the Pt<sub>16</sub>Au<sub>16</sub> NPs may allow Pt to initially concentrate at the silica–NP interface at low temperatures. The low-temperature restructuring would be particularly important for anchoring Au onto silica because Au NPs are mobile on silica surfaces at temperatures as low as 100 °C.<sup>20,51</sup> Continuing work in our lab is aimed at understanding the effects of particle size and composition on this phenomenon, as well as temperature and ligand effects.

**CO Oxidation Catalysis.** Figure 7 shows CO oxidation catalysis data from freshly activated catalysts. The activity of the monometallic Pt<sub>32</sub> catalyst is similar to other dendrimer derived Pt catalysts and to traditional catalysts prepared by wetness impregnation.<sup>34</sup> Under these conditions, Pt shows little activity below 90 °C; above this temperature, activity increases rapidly. The Au<sub>32</sub> catalyst is essentially inactive, consistent with most reports of SiO<sub>2</sub> being inappropriate for preparing active supported Au catalysts.<sup>7,20</sup> The cometallic Pt<sub>32</sub>+Au<sub>32</sub> catalyst has essentially the same features as Pt<sub>32</sub>, except the activity is delayed by about 25 °C, suggesting there may be less surface Pt available for catalysis.

CO oxidation catalysis by Pt<sub>16</sub>Au<sub>16</sub> shows three distinct regions of activity; most notably, there is substantial activity at

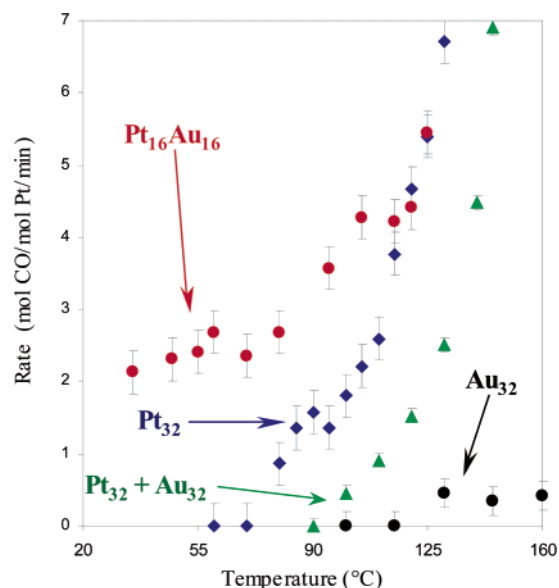


**Figure 7.** CO oxidation catalysis by silica supported Pt<sub>32</sub>, Au<sub>32</sub>, Pt<sub>16</sub>Au<sub>16</sub>Pt, and Pt<sub>32</sub>+Au<sub>32</sub> NPs. Rate is reported as moles CO converted per total moles Pt per minute; for Au<sub>32</sub>, the rate is in moles CO converted per total mole Au per minute.

low temperatures (30–80 °C). We suggest that this activity is due either to Au or possibly to Pt–Au bimetallic sites on the catalyst. At temperatures of 120 °C or higher, the catalyst is indistinguishable from Pt<sub>32</sub> and is consistent with monometallic Pt catalysts.<sup>34</sup> Presumably, surface Pt atoms are very active at these temperatures and are responsible for essentially all of the catalysis. In the intermediate temperature range (80–120 °C, where Pt begins to become active), both metals or types of sites may be active. Alternately, Au may be promoting CO oxidation catalysis by Pt at these temperatures, possibly by breaking up Pt ensembles or providing weak CO or O<sub>2</sub> adsorption sites.<sup>52,53</sup>

Supported Au NPs are well known to be highly active low-temperature CO oxidation catalysts;<sup>7,20,54</sup> however, the most active catalysts utilize reducible oxide supports such as TiO<sub>2</sub>.<sup>7,20</sup> Although the identity of the active catalyst is still under substantial debate,<sup>55</sup> catalytic activity is most commonly associated with the preparation and stabilization of small-metal NPs on the support.<sup>56</sup> The preparation of active Au catalysts is also extremely sensitive to the preparation method employed. Most of the active gold catalysts have been prepared using the “deposition–precipitation” method; however, some other methods (CVD, activation of organometallic complexes) are also suitable for preparing and stabilizing highly dispersed Au NPs on a variety of supports.<sup>7,20</sup> Silica, being mildly acidic and having a low isoelectric point, is unsuitable for the deposition–precipitation method because the surface is negatively charged at pHs required to precipitate Au(OH)<sub>x</sub> on a support. Additionally, silica does not effectively stabilize gold NPs against agglomeration.<sup>20</sup>

Only a few Au/SiO<sub>2</sub> catalysts have been reported to be active near room temperature.<sup>51,57</sup> Schüth et al. deposited auric acid

(46) Bowman, R.; Sachtler, W. H. M. *J. Catal.* **1970**, *19*, 127.

(47) Okamoto, H.; Massalski, T. B. *Bull. Alloy Phase Diagrams* **1985**, *6*, 46–56.

(48) Somorjai, G. A.; Hwang, K. S.; Parker, J. S. *Top. Catal.* **2003**, *26*, 87–99.

(49) Mihut, C.; Chandler, B. D.; Amiridis, M. D. *Catal. Commun.* **2002**, *3*, 91–97.

(50) Chandler, B. D.; Pignolet, L. H. *Catal. Today* **2001**, *65*, 39–50.

(51) Yang, C.-M.; Kalwei, M.; Schuth, F.; Chao, K.-J. *Appl. Catal., A* **2003**, *254*, 289–296.

(52) Bourane, A.; Bianchi, D. *J. Catal.* **2004**, *222*, 499–510.

(53) Fanson, P. T.; Delgass, W. N.; Lauterbach, J. J. *J. Catal.* **2001**, *204*, 35–52.

(54) Lin, S. D.; Bollinger, M.; Vannice, M. A. *Catal. Lett.* **1993**, *17*, 245.

(55) Guzman, J.; Gates, B. C. *J. Am. Chem. Soc.* **2004**, *126*, 2672–2673.

(56) Valden, M.; Lai, X.; Goodman, D. W. *Science* **1998**, *281*, 5383.

(57) Okumura, M.; Nakamura, S.; Tsubota, S.; Nakamura, T.; Azuma, M.; Haruta, M. *Catal. Lett.* **1998**, *51*, 53–58.

onto SBA-15 mesoporous silica that had been functionalized with positively charged groups. Reduction with NaBH<sub>4</sub> yielded supported particles approximately 4.5 nm in diameter; the resulting material had an activity of  $2.7 \times 10^{-4}$  mmol/g<sub>cat</sub>/sec (0.073 mol/mol Au/min) at 30 °C. This catalyst was not thermally stable and began to deactivate at 100 °C. It became completely inactive after 20 min at 160 °C. Haruta et al. have also reported on an Au/SiO<sub>2</sub> catalyst prepared via chemical vapor deposition of the organometallic Au complex (CH<sub>3</sub>)<sub>2</sub>Au(CH<sub>3</sub>COCH<sub>2</sub>COCH<sub>3</sub>). After calcination at 400 °C for 4 h, the average gold NP diameter was  $6.6 \pm 3.8$  nm and the catalyst's activity was approximately  $2 \times 10^{-6}$  mol/g<sub>cat</sub>/sec (0.4 mol CO/mol Au/min) at 30 °C. Closer examination of the PSD for this catalyst indicates a bimodal distribution, with about 15% of the imaged particles smaller than 3 nm.

The Pt<sub>16</sub>Au<sub>16</sub> catalyst is substantially more resistant to particle agglomeration than these materials, having small particles even after treatment at 300 °C for 6+ hours. The activity Pt<sub>16</sub>Au<sub>16</sub> (2 mol CO/mol Au/min at 30 °C, assigning all activity at this temperature to Au) is quite consistent with Haruta's Au/SiO<sub>2</sub> catalyst, with the greater activity of our material coinciding with a greater fraction of particles 3 nm or smaller. It is difficult to unequivocally determine the role of Pt in the low-temperature activity, and it is possible that bimetallic sites are responsible for the catalysis. We favor a simpler explanation in which the primary role of Pt is to help stabilize smaller particles. It is possible that Pt adds additional functionality to the catalyst by not only binding O<sub>2</sub> but also locating bound or activated O<sub>2</sub> near active Au sites. However, the strong binding of CO to Pt on Pt<sub>16</sub>Au<sub>16</sub> and the similar activity to Haruta's Au only material tend to support the premise that the activity is primarily associated with Au. We believe that the Pt<sub>16</sub>Au<sub>16</sub> catalytic behavior is best described by bimetallic NPs in which Au sites are active at low temperatures and Pt sites take over at higher temperatures, when CO is less strongly bound to the surface.

## Summary and Conclusions

Using preformed Cu<sup>0</sup> NPs in hydroxyl terminated PAMAM dendrimers, supported bimetallic Pt–Au NPs within the bulk miscibility gap were prepared. After dendrimer removal, the supported NPs remained small as most were smaller than 3 nm. TEM, EDS, and infrared spectroscopy of adsorbed CO confirmed the bimetallic nature of the NPs. The size and composition of the particles are particularly noteworthy given the propensity of silica supported Au particles to agglomerate during thermal treatments. Infrared spectroscopy of adsorbed CO indicated the presence of Pt and Au sites capable of binding CO. Evidence for a CO adsorbed on Pt in a bimetallic site was suggested by the presence of a strong band at 2050 cm<sup>-1</sup>, consistent with literature precedents. CO desorption experiments also showed anomalous behavior as the Pt–CO band increased in intensity as the Au–CO band intensity decreased. Relative to other silica based catalysts, the supported Pt–Au NPs were highly active CO oxidation catalysts at ambient temperatures.

A model was proposed to help understand the behavior and thermal stability of the bimetallic NPs. The CO desorption data suggests that the NPs have fluxional structures and that strong ligands are capable of drawing Pt to the particle surface at moderate temperatures. We suggest that the strong bonds between surface oxides and platinum effectively concentrate Pt

at the particle–support interface either during deposition or dendrimer removal. This internal migration effectively anchors the bimetallic NPs to the support, reducing their mobility and slowing particle agglomeration processes. The stabilization of small Au NPs appears to be critically important for their catalytic activity when supported on silica. Low-temperature catalytic activity is likely due to catalysis by gold, but bimetallic sites may also play an important role.

## Experimental Section

**Materials.** All solutions were prepared using Nanopure water. Hydroxy-terminated generation 5 starburst polyamidoamine (PAMAM) dendrimers (G5-OH) were obtained as a 5% solution in methanol (Aldrich). Prior to use, methanol was removed by rotary evaporation at room temperature. K<sub>2</sub>PtCl<sub>4</sub>, NaBH<sub>4</sub> and Cu(NO<sub>3</sub>)<sub>2</sub>·xH<sub>2</sub>O were purchased from Aldrich and used as received. HAuCl<sub>4</sub> was obtained from Strem Chemicals. Silica (DAVICAT SI-1403, 245 m<sup>2</sup>/g) was supplied by W. R. Grace. O<sub>2</sub>, H<sub>2</sub>, and He gases are all UHP grade from Airgas. Carbon monoxide (99.8% in aluminum cylinder) was purchased from Matheson Tri-Gas.

**Preparation of Dendrimer-Stabilized Pt and Au Bimetallic Nanoparticles (DSNs).** Dendrimer-stabilized Pt and Au bimetallic NP catalysts were prepared by adapting a literature method.<sup>33</sup> All manipulations were performed under N<sub>2</sub> using standard Schlenk techniques. Twenty milliliters of G5-OH (0.01 mM) was mixed with 1.6 mL Cu(NO<sub>3</sub>)<sub>2</sub> (5 mM) at pH 7.0–7.5 and degassed for 20 min. A 3-fold molar excess of NaBH<sub>4</sub> was added to prepare (G5-OH(Cu)<sub>40</sub>) nanocomposites. After 30 min, the pH of the resulting brown solution was adjusted to 3.0 with HClO<sub>4</sub> and stirred for 1 h. Solutions of K<sub>2</sub>PtCl<sub>4</sub> (0.64 mL, 5 mM) and HAuCl<sub>4</sub> (1.6 mL, 2 mM) were degassed separately, mixed, and immediately added to the G5-OH(Cu)<sub>40</sub> nanocomposite solution. The mixed solution was stirred for an additional 1–2 h and deposited onto the solid supports (see below).

The synthesis of dendrimer-stabilized Pt or Au monometallic NPs by Cu displacement was similar to the above method. For Pt<sub>32</sub>, 0.2 μmol G5-OH(Cu)<sub>32</sub> nanocomposites were prepared, and 1.28 mL (5mM) of K<sub>2</sub>PtCl<sub>4</sub> solution was added to prepare Pt<sub>32</sub> NPs. To make Au<sub>32</sub> NPs, 3.2 mL (2mM) of HAuCl<sub>4</sub> solution was mixed with 0.2 μmol G5-OH(Cu)<sub>48</sub>. In all cases, the NPs were immediately deposited onto the support.

**Deposition and Activation.** The resulting DSNs were deposited onto silica support via slow adsorption. The pH of DSN solution was adjusted to 8.5–9, SiO<sub>2</sub> was added, and the suspension was stirred overnight. The resulting dark solid was separated from the colorless mother liquor with a fine frit. The wet solid catalysts were stirred with saturated EDTA solution at pH 7.0–8.0 for 15–20 min and then filtered and washed with deionized water. The EDTA wash was repeated three times. The catalyst was washed several times with deionized water and dried in a vacuum oven at 50 °C overnight. The yields of Pt and Au DSNs were generally about 70–75% and Cu residual was always less than 0.01%. Supported DSNs were activated as described previously (300 °C for 4 h under O<sub>2</sub> followed by 300 °C under H<sub>2</sub> for 2 h).<sup>34</sup>

**Pt and Au analysis with Atomic Absorption Spectroscopy.** Pt and Au loadings on catalysts were determined with a Varian SpectrAA 220FS atomic absorption spectrometer using an acetylene/air flame, as described previously.<sup>34</sup> Briefly, the sample was treated with freshly prepared aqua regia and the pH was adjusted to 6.0–7.0 with ammonium hydroxide. The resulting solution was condensed and transferred to a 10-mL volumetric flask containing sufficient La(NO<sub>3</sub>)<sub>3</sub> to yield a final solution of 1% La. AA standards were prepared from Aldrich AA standard solutions and deionized water.

**In-Situ FT-IR Experiments.** FTIR spectra were collected using a Thermo Nicolet Nexus 470 spectrometer equipped with a DTGS detector with a resolution of 2 cm<sup>-1</sup>. A water-cooled stainless steel IR flow cell with NaCl windows was used to hold a pressed catalyst wafer

(17–19 mg). The optical bench and beam path (outside the flow cell) were continuously purged with N<sub>2</sub>. A heating element wrapped around the cell with a thermocouple placed in close proximity to the catalyst sample allowed for in-situ heating of samples and collection spectra at different temperatures. All spectra were collected with gases flowing at 30 mL/min. Gas composition was manipulated by adjusting rotameters on an external manifold.

CO adsorption experiments were carried out after in-situ reduction (20% H<sub>2</sub>/He at 300 °C for 2 h) and flushing with He for 1 h at 300 °C. Samples were then cooled under He flow to room temperature and a background spectrum was collected. A 5% CO/He mixture was flowed over the sample for 15 min, followed by pure He. IR spectra of CO adsorbed on the catalyst surface were collected after all the gas-phase CO had been purged from the sample. CO desorption was accomplished by heating the sample under flowing He.

**CO Oxidation Catalysis.** CO oxidation experiments were performed as described previously.<sup>34</sup> Briefly, diluted 20 mg of catalyst was diluted with  $\alpha$ -Al<sub>2</sub>O<sub>3</sub> and placed in a single pass plug flow microreactor. Catalytic activity used a feed composition of 1.1% CO and 20% O<sub>2</sub>. Feed and reactor effluent composition was measured via gas chromatography using a TCD detector. Consequently, the feed flow rate was held constant at 26 mL/min (space velocity 75 000 hr<sup>-1</sup>) and conversion was measured as a function of temperature. Rate data was determined only when conversion was less than 10%.

**TEM and EDS Analysis.** SiO<sub>2</sub>-supported catalysts were suspended in dichloroethane and sonicated for 5 min. TEM samples were prepared

by placing a drop of the suspension on a copper grid (200 mesh, PELCO) with a thin carbon coating. Transmission electron microscopy (TEM) was performed on a JEOL 2010F operating at 200 kV equipped with an INCAEnergyTEM EDS System with a 30 mm<sup>2</sup> Li drifted detector calibrated using the zero loss and Cu K and L lines. EDS spectra for individual particles were collected with a 0.5-nm beam diameter for an acquisition time of 2 min. EDS data was treated using the Cliff–Lorimer quantitation method.<sup>58</sup>

**Acknowledgment.** We gratefully acknowledge the Robert A. Welch Foundation (Grant Number W-1552) for financial support of this work. Acknowledgement is made to the donors for the American Chemical Society Petroleum Research Fund for partial support of this research. We also thank Prof. D. Wayne Goodman and Prof. Richard M. Crooks from Texas A&M University for their input and helpful discussions.

**Supporting Information Available:** Representative TEM micrographs and TEM particle size distributions for all catalysts. Representative EDS spectrum for Pt<sub>16</sub>Au<sub>16</sub>; IR spectrum of Au<sub>32</sub> after treatment with CO and flushing with He. This material is available free of charge via the Internet at <http://pubs.acs.org>.

JA046542O

---

(58) Cliff, G.; Lorimer, G. W. *J. Microsc.* **1975**, *103*, 179.